The Flexural Mechanics of Creased Thin Strips

M.G. Walker[a,1,*], K.A. Seffen[a]

[a] *Cambridge University Engineering Department, Trumpington St, Cambridge, United Kingdom, CB2 1PZ*

Abstract

Many structures in Nature and Engineering are dominated by the influence of folds. A very narrow fold is a crease, which may be treated with infinitesimal width for a relatively simple geometry; commensurately, it operates as a singular hinge line with torsional elastic properties. However, real creases have a finite width and thus continuous structural properties. We therefore consider the influence of the crease geometry on the large-displacement flexural behaviour of a thin creased strip. First, we model the crease as a shallow cylindrical segment connected to initially flat side panels. We develop a theoretical model of their coupled flexural behaviour and, by adjusting the relative panel size, we capture responses from a nearly singular crease up to a full tape-spring. Precise experiments show good agreement compared to predictions.

Keywords: Creasing, Folding, Shell structures, Tape-spring

*Corresponding author

Email addresses: martin.walker@some.ox.ac.uk (M.G. Walker), kas14@cam.ac.uk (K.A. Seffen)

[1]Present affiliation: Department of Engineering Science, University of Oxford, Parks Road, Oxford, United Kingdom, OX1 3PJ.

1. Introduction

We investigate the flexural behaviour of a thin creased strip. A crease is the sharp ridge which forms between flat, inclined side panels when a flat strip is folded along its length. Their bending provides insight into the mechanics of more elaborate sheets with patterns of folds and creases, such as insect wings [1, 2], pleated fabric [3], and Origami metamaterials [4].

Creasing increases the structural depth of the original strip without adding extra material, in the same way that distributed curving performs in a regular carpenter's tape, or "tape-spring" [5, 6, 7, 8]. The cross-sections of very thin strips, however, begin to flatten during moderate bending along their length, which subtracts from their initial bending stiffness.

During so-called "equal-sense" bending [9] the outside edges of the strip become compressed and buckle asymmetrically, leading to twisting along the strip. Eventually the buckles coalesce into a single cylindrical fold region connected to virtually undistorted parts on both sides, see Fig. 1. More of the folded strip becomes enveloped longitudinally when the ends are rotated further and *vice versa*.

The same type of performance and shape of fold is also observed when ordinary tape-springs are bent similarly. The cross-section of the folded creased strip, however, is not entirely smooth. A cross-sectional profile in Fig. 1 shows the horizontal side panels connected in the middle by a visible remnant of the original crease.

When the direction of bending is reversed to give "opposite-sense" behaviour, the strip collapses into a pronounced vertex, Fig. 2. This is a quite different localised response: the shape of the vertex remains the same when

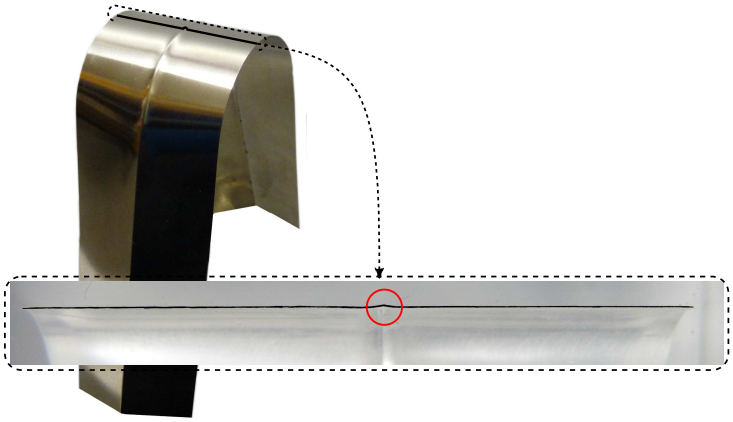

Figure 1: Equal-sense bending of a creased strip. A cross-section through the crease is made by setting the folded strip in resin, sawing in half and then polishing to reveal the persistence of the original crease as a small but distinguishable raised central feature.

Figure 2: Opposite-sense bending of creased strip, leading to a bistable vertex.

the end rotations are increased, and it may remain in place after unloading to give *bistable* behaviour [9]. It is also different from opposite-sense bending of tape-springs, which produces another folded cylindrical region.

A large-displacement analysis must therefore treat the creased strip as a shell structure. The challenge is then how to model the strip entirely, for the crease is concentrated in width compared to the panel size. In the limit, the crease may be conferred as an elastic line separating deformable panels. Any opening or closing across the crease itself is achieved by a relative rotation of the side panels, with resistance provided by a torsional spring (per unit length of crease).

This simplifies any potential kinematical specification but, paradoxically, prevents any theoretical determination of stiffness. Careful experiments must be performed, for example, by pulling the crease apart via the side panels and converting the measured force and transverse displacement into an elastic torque-rotation characteristic in this direction [10, 11, 12, 13].

Other techniques in a range of materials are described by [13, 14, 15, 16], where the panel deformation has to be subtracted from overall levels, to quantify the crease alone. From analysis of the relative contributions from the panels and crease, Lechenault et al. [12] also identify an upper limit on the size of panel with negligible deformations: any panel with smaller proportions behaves as if it were rigid compared to the crease. Origami sheets, for example, which comply with the same limit on spacing between fold-lines, behave kinematically as rigid-folded mechanisms.

The same torsional spring characteristic applies to opening (and closing) of a crease during longitudinal bending, where the dominant in-plane forces are now longitudinal. The nature of deformation and thence the coupling between the crease and panels now changes compared to the qualifying experiments.

Very thin panels may respond in a *developable* manner. In-plane forces can be neglected altogether, and the coupled structural response relies on finding compatible conical displacement fields with the crease line performance; for example, Dias et al. [17, 18] present a general methodology which includes creased strips with a curved centreline.

We do not ordain the crease as a singular spring but are inspired by its remnant in Fig. 1 being a small tape-spring element, which can bend and

stretch longitudinally. The equilibrium response of the side panels is the same, with matching shear forces and bending moments at the connecting edges, where compatible deformations must also be observed. Each panel width is no more than one tenth of strip length, in order to exclude transverse in-plane forces altogether.

Uniform changes in longitudinal curvature are assumed for tractability, reducing the analysis to the mechanics of a cross-section of unit length, as per ordinary tape-spring analysis [19] and Brazier's analysis of the ovalisation of bent tubes [20]. This precludes knowledge of the transition between localised flattened and undeformed regions and consequently the corresponding end rotations. The transitional behaviour of deformed thin shells has been investigated for simpler geometries [21, 22]; a comparable analysis for creased strips, and tape-springs, is a formidable challenge which we do not tackle here. The general uniform curvature solution, nonetheless, allows us to examine mechanical behaviour of the strip and the nature of an equivalent torsional spring furnished by the crease region.

Our large-displacement analysis does not capture directly any localised behaviour because of the uniform curvature specification. However, the progression of localised deformation in Fig. 1 mirrors a *propagating instability* of fixed shape, which has been used to classify the folded behaviour in ordinary tape-springs [23]. Submitting the uniform large-displacement response to the so-called *Maxwell construction* reveals the exact folded properties provided the response path has an "up-down-up" character *i.e.* the moment resistance peaks, then softens, before rising again with increasing end rotation.

The propagating shape of the folded region has a fixed longitudinal cur-

vature and changing arc-length. The opposite-sense concentrated shape of Fig. 2 does not conform and thus cannot be classified using Maxwell's scheme. Better alternatives assume a developable shape around the vertex [9, 13], so we focus on equal-sense behaviour alone.

Given that our tape-spring elements are very small compared to the overall width of the strip, the sensitivity of any Maxwell conformity to the size of tape is thus interesting to study. We therefore allow the tape to become relatively large, even removing the panels altogether so that we confirm ordinary tape-spring behaviour at the end of our assessment range.

For consistency, we make strips with these "distributed" creases and observe whether or not longitudinal folding behaves in a propagating manner; we also simulate their bending using finite element analysis and compare results. Even though quantifying the equivalent torsional spring is a primary aim, this is only strictly true for very small tape-spring elements: how the spring develops for larger tape elements is merely instructive but interesting. Other features worth studying are the initial stiffness, the peak moment, the curvature of the folded region, and so forth. The layout is as follows:

In the following section, we derive a model of the coupled flexural response for large displacements. Most of the analysis is presented in closed form although some of the final expressions have many terms and cannot be. A range of response predictions is given for strips of a fixed arc-width and differently sized tape-spring elements.

We consider first the transverse curvature change on the centre-line of the crease for a sense of how much it opens. Peak axial strains are then calculated in view of material yielding. The non-linear moment-curvature response and

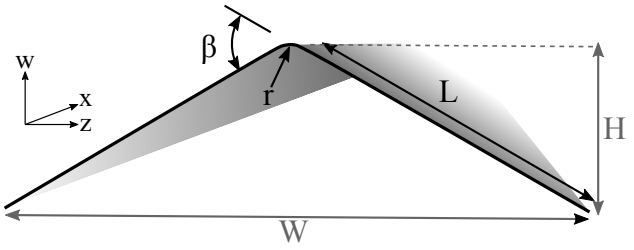

Figure 3: Idealised cross-section of a creased strip. L is the panel length, r is the tape-spring element radius, β is the initial strip sector angle, H is the apex height and W is the edge-to-edge width.

opening angle are computed before quantifying the spring characteristic.

We then formally consider the localised folded region as a propagating instability. Simple predictions of propagating moment and curvature are calculated and compared in Section 5 to experiments described in Section 3 and to finite element analysis laid out in Section 4. This study then concludes.

2. Analysis

Consider a tape-spring joined smoothly to identical flat panels on its edges, forming the cross-section shown in Fig. 3, with initial transverse radius r, panel width L, and sector angle β. A global coordinate system (x, z, w) is specified, where x lies along the unit length of the strip, z is transverse, and w is normal and vertical to the tape-spring centre-line. The strip has a uniform thickness t.

End effects are neglected, there are no applied surface loads, nor residual stresses. Uniform longitudinal curvature, denoted by κ_x, is assumed. We also neglect torsional deformations by assuming symmetrical deformation about the centre-line of the strip; they do not affect the shape and properties of the localised folded region that forms later.

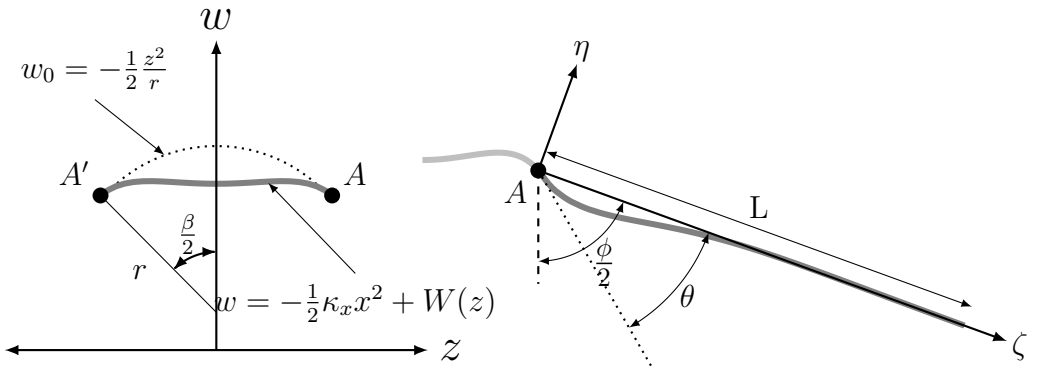

(a) Deformed tape-spring geometry.

(b) Deformed side panel geometry.

Figure 4: Analytical cross-section. Dotted lines show the initial geometry; points A and A' indicate the locations where the tape-spring and panel geometry are connected.

We now separate the tape-spring crease, Fig. 4a, from the side panels, Fig. 4b, which are connected at points A and A' by compatible deformations. Their coupled deformation is described by two degrees of freedom, κ_x, and the opening angle, ϕ, across the tape-spring.

The equilibrium cross-sectional shape of the strip due to the imposed uniform longitudinal curvature κ_x is found using a variational approach. We write a general expression for the strain energy density per unit length of the strip, whose first variation is zero at equilibrium. The governing differential equations for the deformation of the crease and panel regions are then solved subject to compatibility constraints at the crease-panel interface.

The strain energy density due to bending is

$$u_B = \frac{D}{2}\left[(\kappa_1 + \kappa_2)^2 - 2(1-\nu)\kappa_1\kappa_2\right] \tag{1}$$

where κ_1 and κ_2 are the changes in principal curvatures [24], $D = Et^3/12(1-$

ν^2) is the flexural rigidity, E is Young's modulus, and ν is Poisson's ratio. The strain energy density due to stretching in terms of principal in-plane stress resultants, N_1 and N_2, is written as

$$u_S = \frac{1}{2Et}\left[(N_1+N_2)^2 - 2(1+\nu)N_1N_2\right] \tag{2}$$

Since we assume zero transverse stress ($N_2 = 0$), the above depends only on the longitudinal stress resultant in both the tape and the panels, $N_1 = N_x = Et\kappa_x y$, with y measuring the vertical distance of a point on the strip cross-section from the neutral axis.

The initial cross-section of the tape-spring element is shallow and approximately parabolic [19] with $w_0 = -z^2/2r$, see Fig. 4a. The deformed cross-section is specified by $w = -\kappa_x x^2/2 + W(z)$, where $W(z)$ is an unknown symmetrical function defining the crease shape relative to the strip neutral axis in the vertical direction: thus $W(z)$ is equivalent to y. The bending and stretching energies of the crease are therefore:

$$(u_B)_C = \frac{D}{2}\left[\left(\frac{\partial^2 W}{\partial z^2} + \kappa_x - \frac{1}{r}\right)^2 - 2\kappa_x(1-\nu)\left(\frac{\partial^2 W}{\partial z^2} - \frac{1}{r}\right)\right] \tag{3}$$

$$(u_S)_C = \frac{Et{\kappa_x}^2}{2}W^2 \tag{4}$$

The intrinsic panel (η, ζ) coordinate system is initially aligned tangentially to the tape-spring edge at A (and reflected vertically for A'). During deformation, the ζ axis rotates by an angle θ from the tape-spring edge tangent, shown dotted in Fig. 4b, to an angle $\phi/2$ from vertical. The angle ϕ is thus the *asymptotic* opening angle of the strip since it measures the axis in-

clination and not the local deformation of the panel. When the cross-section has flattened, ϕ will approximately equal π.

We assume the panel region deforms by $\eta(\zeta)$ relative to the ζ axis with a longitudinal curvature equal to the projection of the strip curvature, κ_x, onto the same axis. The panel edge at A (and A') is rotated by θ to ensure gradient compatibility with the tape-spring crease. Assuming zero in-plane stress in the ζ direction, the panel deformation energy is:

$$(u_B)_P = \frac{D}{2}\left[\left(\frac{d^2\eta}{d\zeta^2}\right)^2 + \left(\kappa_x \sin\frac{\phi}{2}\right)^2 + 2\nu\frac{d^2\eta}{d\zeta^2}\kappa_x \sin\frac{\phi}{2}\right] \tag{5}$$

$$(u_S)_P = \frac{Et\kappa_x^2}{2}\left(\eta\sin\frac{\phi}{2} + \zeta\cos\frac{\phi}{2} + W(A)\right)^2 \tag{6}$$

The squared term in Eqn 6 is the panel deformation transformed to the strip coordinate system and $W(A)$ is the crease deformation evaluated at the crease-panel interface, A.

The total strain energy per unit length of the strip is therefore

$$U = 2\int_0^{r\sin\frac{\beta}{2}} \left[(u_S)_C + (u_B)_C\right] dz + 2\int_0^L \left[(u_B)_P + (u_S)_P\right] d\zeta \tag{7}$$

This is subject to the cross-section equilibrium conditions:

$$\int_{width} N_x z \; dz = 0 \qquad\qquad \int_{width} N_x \; dz = 0 \tag{8}$$

The first of these conditions is satisfied since we have assumed symmetric deformations about the strip centreline. These deformations must also satisfy the second equilibrium constraint in Eqns 8, which is enforced using a Lagrange multiplier, λ. Forming the Lagrangian using Eqn 7 and the second

of Eqns 8:

$$\mathcal{L} = U + \lambda E t \kappa_x \left[\int_0^{r \sin \frac{\beta}{2}} W dz + \int_0^L \left(\eta \sin \frac{\phi}{2} + \zeta \cos \frac{\phi}{2} + W(A) \right) d\zeta \right] \quad (9)$$

The governing differential equations for the crease, W, and panel, η, deformation are now obtained by setting the first variation of Eqn 9 to zero:

$$\frac{1}{4\gamma^4} \frac{\partial^4 W}{\partial z^4} + W = -\frac{\lambda}{\kappa_x} \quad (10)$$

$$\frac{1}{4\gamma^4} \frac{\partial^4 \eta}{\partial \zeta^4} + \eta \sin^2 \frac{\phi}{2} = -\frac{\zeta}{2} \sin \phi - W(A) \sin \frac{\phi}{2} - \frac{\lambda}{\kappa_x} \sin \frac{\phi}{2} \quad (11)$$

where $\gamma^4 = 3\kappa_x^2 \left(1 - \nu^2\right) / t^2$. Solving Eqns 10 and 11 the deformed shapes of the crease and panel are obtained:

$$W = C_1 \cos \gamma z \cosh \gamma z + C_2 \sin \gamma z \sinh \gamma z + C_3 \quad (12)$$

$$\eta = \frac{\theta}{\gamma^*} e^{-\zeta \gamma^*} \sin \left(\zeta \gamma^* \right) \quad (13)$$

where

$$C_3 = -\frac{\lambda}{\kappa_x} = \frac{\kappa_x}{2(\gamma L + \Omega)} \left[\frac{\theta}{\gamma} e^{-\gamma^* L} \left(\sin \left(\gamma^* L \right) + \cos \left(\gamma^* L \right) \right) - \frac{\theta}{\gamma} - L^2 \gamma \cos \frac{\phi}{2} \right.$$
$$\left. - \cosh \Omega \left(\left(C_1 + C_2 \right) \sin \Omega + 2\gamma C_1 L \cos \Omega \right) + \sinh \Omega \left(\left(C_2 - C_1 \right) \cos \Omega - 2\gamma C_2 L \sin \Omega \right) \right]$$

with $\Omega = \gamma r \sin \left(\beta / 2 \right)$ and $\gamma^* = \gamma \sqrt{\sin \left(\phi / 2 \right)}$. Constants C_1 and C_2, and the panel edge rotation θ, are determined from compatibility of gradient, bending moments, and out-of-plane shear forces at the tape-panel interface.

Compatibility of shear forces provides an expression for the panel edge rotation, θ:

$$\frac{\partial^3 W}{\partial z^3} = \frac{\partial^3 \eta}{\partial \zeta^3} \frac{1}{\sin \frac{\phi}{2}} \quad \longrightarrow \quad \theta = \frac{1}{2\gamma^2} \left(\frac{\partial^3 W}{\partial z^3} \right) \quad (14)$$

The gradient and bending moment compatibility equations are

$$\frac{\partial W}{\partial z} = \tan\left(\frac{\pi}{2} - \frac{\phi}{2} + \theta\right) \approx \cot\frac{\phi}{2} + \theta\left(1 + \cot^2\frac{\phi}{2}\right) \tag{15}$$

$$\frac{\partial^2 W}{\partial z^2} - \frac{1}{r} + \nu\kappa_x = \frac{\partial^2 \eta}{\partial \zeta^2}\frac{1}{\sin\frac{\phi}{2}} + \nu\kappa_x \sin\frac{\phi}{2} \tag{16}$$

where Eqn 15 uses the Maclaurin series in θ and neglects higher-order terms. Substituting Eqn 14 into Eqns 15 and 16, we arrive at

$$\gamma^*\left(\frac{\partial^2 W}{\partial z^2} - \frac{1}{r}\right) + \frac{\partial^3 W}{\partial z^3} + \nu\kappa_x\gamma^*\left(1 - \sin\frac{\phi}{2}\right) = 0 \tag{17}$$

$$2\gamma^2 \sin\frac{\phi}{2}\left(\sin\frac{\phi}{2}\frac{\partial W}{\partial z} - \cos\frac{\phi}{2}\right) - \frac{\partial^3 W}{\partial z^3} = 0 \tag{18}$$

which provide the boundary conditions to solve for the unknown constants C_1 and C_2. After some lengthy calculation, we find

$$\begin{aligned} C_1 G = &-2\cos\Omega\sinh\Omega\cos^2\frac{\phi}{2}\left(\kappa_x\nu\sin\frac{\phi}{2} - \kappa_x\nu + \frac{1}{r}\right) + 4\gamma^*\cos\frac{\phi}{2}\left(\sin\Omega\cosh\Omega - \cos\Omega\sinh\Omega\right) \\ &- \cosh\Omega\left(\sin\Omega(3 - \cos\phi)\left(\kappa_x\nu\sin\frac{\phi}{2} - \kappa_x\nu + \frac{1}{r}\right) - 2\gamma\cos\Omega\sin\phi\right) \end{aligned} \tag{19}$$

$$\begin{aligned} C_2 G = &-2\sin\Omega\cosh\Omega\cos^2\frac{\phi}{2}\left(\kappa_x\nu\sin\frac{\phi}{2} - \kappa_x\nu + \frac{1}{r}\right) - 4\gamma^*\cos\frac{\phi}{2}(\cos\Omega\sinh\Omega + \sin\Omega\cosh\Omega) \\ &+ \sinh\Omega\left[\cos\Omega(\cos\phi - 3)\left(\kappa_x\nu\sin\frac{\phi}{2} - \kappa_x\nu + \frac{1}{r}\right) - 2\gamma\sin\Omega\sin\phi\right] \end{aligned} \tag{20}$$

where

$$G = \gamma^2\left[4\cos 2\Omega\sin^{\frac{3}{2}}\frac{\phi}{2} - 4\cosh 2\Omega\sin^{\frac{3}{2}}\frac{\phi}{2} - \sin 2\Omega\left(\cos\phi + 1\right) + \sinh 2\Omega\left(\cos\phi - 3\right)\right]$$

As these confirm, $W(z)$ and the panel displacement, $\eta(\zeta)$, only depend on

the initial strip geometry, the longitudinal curvature, κ_x, and the asymptotic opening angle, ϕ.

Due to the lengthy closed-form solution of Eqn 7, it is minimised for a particular value of κ_x to obtain ϕ using a numerical scheme in Mathematica [25]. The corresponding cross-sectional shape of strip is obtained by substituting κ_x and ϕ into Eqns 12 and 13, which is repeated for the range of values of κ_x. The end moments applied to the strip are obtained by differentiating Eqn 7 with respect to the strip curvature κ_x [24] and then substituting the opening angle ϕ.

2.1. Model predictions

Certain predictions are shown in Fig. 5. All strips have a width of cross-section equal to $\beta r + 2L = 41t$, a sector angle $\beta = 60°$, and initial tape-spring radii, r, ranging from $4t$ to $39t$, with the last value corresponding to a full tape-spring ($L = 0$). While the smaller crease radii are outside the normally accepted range for thin-shell theory, this ultimately has little effect on the results since the crease does not open significantly when the radius is small [26, 27]. The strip curvature, κ_x, and radius, r, are made dimensionless using the strip thickness, t, and bending moments by the shell rigidity, D.

Because the transverse curvature changes within the tape-spring are not uniform, we use the value at the centre of the strip ($z = 0$). From Eqn 12, $\kappa_z = \partial^2 W/\partial z^2|_{z=0} = 2C_2\gamma^2$. The ratio of this transverse curvature to the initial tape curvature is plotted in Fig. 5a for increasing values of strip curvature.

When the initial tape radius is reduced, the change in its curvature becomes smaller, indicating that smaller creases open less. Because the tape-

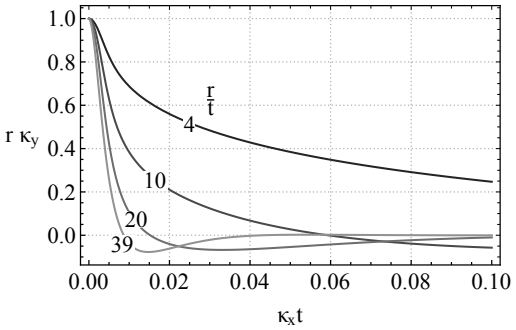

(a) Curvature at tape-spring centre ($z = 0$)

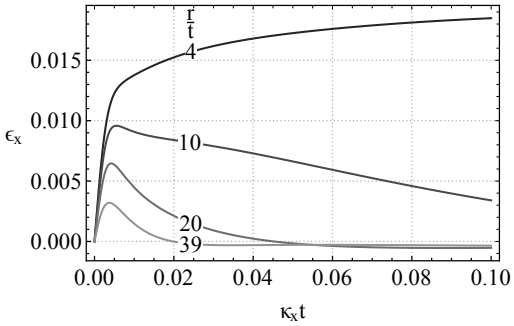

(b) Longitudinal strain at tape-spring centre ($z = 0$)

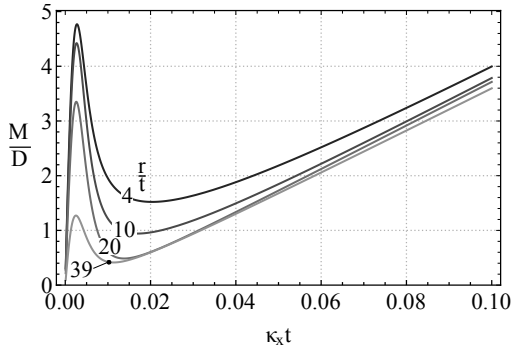

(c) Applied end moment *vs* curvature

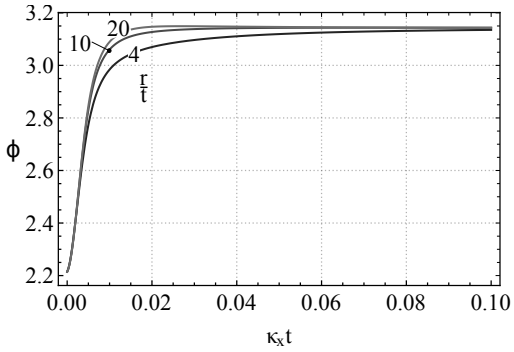

(d) Asymptotic opening angle *vs* curvature

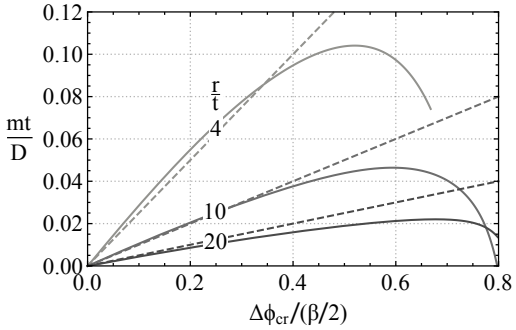

(e) Equivalent crease spring opening behaviour

Figure 5: Theoretical behaviour. Each strip has a total arc-width $r\beta + 2L = 41t$, $\beta = 60°$ and $\nu = 0.3$. As the tape-spring radius is reduced, the strip opens less and the bending resistance increases. Note that the $r/t = 39$ curve corresponds to a full tape-spring ($L = 0$).

spring can deform non-uniformly, the curvature oscillates about zero over the width of tape for larger r, resulting in locally negative curvatures, seen for $r/t = 10$, $r/t = 20$, and $r/t = 39$.

The longitudinal strain, ϵ_x, at the centre of the strip ($z = 0$) is shown in Fig. 5b. For larger r/t, the strain peaks as the strip flattens, before decreasing. For smaller r/t, this peak disappears and the strain increases monotonically as a result of the larger structural depth due to the prominence of the crease. The peak strain attained by the strips shown in Fig. 5b can be larger than the yield strain of typical metals, leading to local damage.

The moment-curvature behaviour is shown in Fig. 5c, which repeatedly shows an up-down-up shape, even for the smallest tape-spring element—as we surmised for a propagating instability behaviour. Each strip has a different initial stiffness because they have the same arc-width but different second moments of area. For very large strip curvatures, the slope of the moment-curvature curve approaches the same value as a plate of width equal to the arc-width ($\beta r + 2L$). For smaller r/t, there is less opening and hence flattening of the tape-spring element even though the overall cross-section becomes largely flat, *c.f.* Fig. 1. The reduction in the initial structural depth is limited, setting a higher moment profile in general. By focusing the tape into a smaller region, the bending resistance is increased while keeping the same cross-sectional width.

The asymptotic opening angle, ϕ, is shown in Fig. 5d. Initially, when $\kappa_x = 0$, $\phi = 2.2 \approx 126^\circ$ despite $\beta = 60^\circ$, which should set $\phi = \pi - \beta = 120^\circ$. This initial difference is caused by the original cross-section of the tape-spring element not being sufficiently shallow, but which decreases as β is reduced.

In Fig. 5d, however, the cross-section quickly flattens with increasing strip curvature, but more slowly as the crease radius is decreased.

2.2. Torsional spring

In other studies, the specified torsional spring applies an edge moment to the panel as a function of the crease opening angle. In order to obtain an equivalent torsional spring, we extract the moment and corresponding rotation at the tape-panel interface as the strip bends. Using the right-hand side of the curvature compatibility statement, Eqn 16

$$\frac{mt}{D} = \frac{-2\gamma^{*}\theta}{\sin\left(\phi/2\right)} + \kappa_x \nu \sin\frac{\phi}{2} \tag{21}$$

Similarly, the angle of inclination at the interface can be obtained from the slope compatibility equation

$$\tan\phi_{cr} = \cot\frac{\phi}{2} + \theta\left(1 + \cot^2\frac{\phi}{2}\right) \tag{22}$$

The change in crease angle is $\Delta\phi_{cr} = \phi_{cr}\left(\kappa_x\right) - \phi_{cr}\left(0\right)$ and thus, the equivalent torsional spring response is set by $m = k_{\text{eff}}\Delta\phi_{cr}$, where k_{eff} is the opening stiffness. The effect of shear at the crease-panel interface is neglected since it is small for shallow creases.

The crease opening behaviour is shown in Fig. 5e. Generally, the opening resistance increases as the initial radius is decreased; it is also non-linear, with the stiffness gradually decreasing as $\Delta\phi_{cr}$ increases.

An approximate expression for the opening behaviour of the crease can be obtained by assuming a constant curvature response of the tape-spring

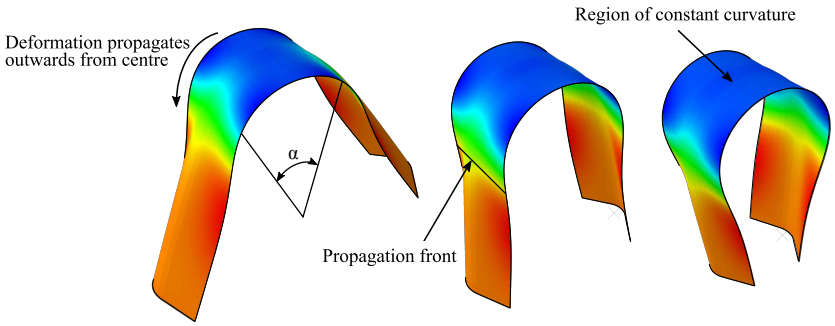

Figure 6: Contours of constant longitudinal curvature for increasing end rotations of strip from finite element analysis, Section 4. The angle α indicates the sector angle of the central folded region.

element [27]:

$$\frac{mt}{D} = \frac{2\Delta\phi_{cr}}{\beta r} \tag{23}$$

This is shown as dashed lines in Fig. 5e. These match the opening resistance from the analytical model well for small crease opening angles ($\Delta\phi_{cr}$) but over-estimate the opening resistance at large angles. Equation 23 therefore provides a reasonable linear spring approximation for small-to-moderate crease opening angles.

2.3. Propagation of deformation

Experiments presented later show that the folded deformation of a highly bent strip proceeds without a significant change in bending resistance. The series of simulated shapes from finite element analysis in Fig. 6 clearly show the folded region growing in length along the strip but not changing its radius of curvature.

This propagating form of deformation has been studied for various structures including the collapse of undersea pipelines [28, 29] and long shallow panels [30], the deformation of beams on non-linear elastic foundations [31],

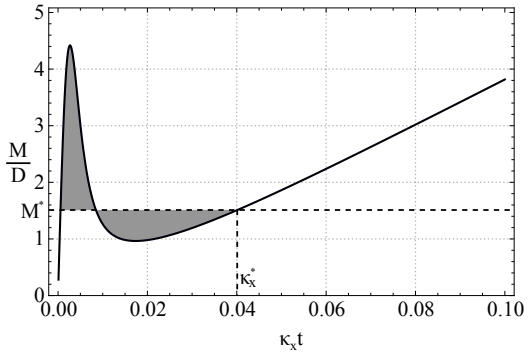

Figure 7: Moment-curvature behaviour for the strip with $r/t = 10$ in Fig. 5c. The propagation moment, M^*, is determined by finding a line which equates the enclosed areas above and below it (shown shaded). The curvature associated with the third crossing of this line is the propagation curvature, κ_x^*.

the inflation of elastic tubes [28], and the collapse of buildings [32]. Kyriakides [33] provides a detailed discussion of the analysis of this phenomenon.

The load-deformation behaviour exhibited by such structures must feature an intermediate reversal of gradient—the up-down-up (or alternatively down-up-down) shape. This is clearly exhibited in the moment-curvature responses in Fig. 5c, and the applied end moments required to sustain this are obtained using Maxwell's construction. This is an energy argument based on the path independence of strain energy [28, 23], which implies:

$$\int_{\alpha_0}^{\alpha^*} M d\alpha - M^* (\alpha^* - \alpha_0) = 0 \tag{24}$$

where α is the longitudinal sector angle of the flattened region in Fig. 6, and α_0 and α^* are the first and third intersections respectively of the horizontal line M^* and the $M(\alpha)$ curve. The constants M^* and α^* correspond to the unknown propagating equilibrium configuration which solves Eqn 24.

Since our model assumes uniform curvature, κ_x, along the length of the

strip, then $\alpha = \kappa_x s$ for an arbitrary length s, and $M(\alpha)$ differs from $M(\kappa_x)$ only by a scale factor [23]. Setting s equal to unity, the propagating moment, M^*, is found by equating the areas above and below the horizontal line, $M = M^*$, shown shaded in Fig. 7. The curvature (*viz.* rotation) associated with this propagation, $\alpha^* = \kappa_x^*(1)$, is obtained from the third intersection point by numerical integration.

Approximate values for M^* and κ_x^* can be found by assuming that the crease flattens completely to give a purely cylindrical longitudinal fold. The change in transverse curvature in the tape-spring is then $1/r$, with none in the side panels; both experience a change in longitudinal curvature of κ_x.

Since there is no stretching, only bending strain energy has to be considered, which is minimised at $\kappa_x = \kappa_x^*$ for the propagating case. The total bending strain energy multiplies the bending energy density, Eqn 1, by the surface area of the folded tape-spring, $\beta r\alpha/\kappa_x$, and the panels, $L\alpha/\kappa_x$:

$$U = D\alpha \left[\frac{\beta}{2} \left(r\kappa_x + \frac{1}{r\kappa_x} - 2\nu \right) + L\kappa_x \right] \tag{25}$$

Thus

$$\frac{1}{\kappa_x^*} = r\sqrt{\frac{2L}{\beta r} + 1} \tag{26}$$

The equivalent propagating moment is obtained by differentiating Eqn 25 with respect to α and substituting Eqn 26

$$\frac{M^*}{D} = \beta \left(\sqrt{\frac{2L}{\beta r} + 1} - \nu \right) \tag{27}$$

When L is set to zero, M^* and κ_x^* equal the well-known propagating moment and curvature for ordinary tape-springs under equal-sense bending [23].

Equations 26 and 27 can also be combined into a single expression using $2L = S - \beta r$, where S is the arc-width of the strip. Eliminating r between them, we find

$$M^* = D(\kappa_x^* S - \beta\nu) \tag{28}$$

The ranges of validity of Eqns 26 and 27 are considered in Section 5.

3. Experimental set-up

Creased metallic strips were made from 0.12 mm thick copper beryllium sheet with a Young's modulus of 131 GPa and Poisson's ratio of 0.3. Strips with a width of 50 mm and length of 350 mm were clamped and thus bent into a creased shape in a heavy mould. The mould had four serrated ridges all subtending 60° but with different radii, from 1 mm to 10 mm.

The clamped strips were age-hardened at 330°C in a commercial oven for five hours. They opened slightly after removal from the mould due to precipitate migration through the thickness during heat treatment; this is similar to well-known elastic spring-back. To determine their formed geometries accurately, their external edge-to-edge widths, W, and apex heights, H, were measured (Fig. 3). Parameters r, L, β, in Table 1 were then calculated by solving

$$\beta r + 2L = 50 \text{ mm} \quad L\sin\frac{\beta}{2} + r\left(1 - \cos\frac{\beta}{2}\right) = H \quad 2L\cos\frac{\beta}{2} + 2r\sin\frac{\beta}{2} = W \tag{29}$$

The ends of the cooled strips were cast in polyurethane resin blocks, for later connection to the bending test apparatus shown in Fig. 8 and described in detail in [26]. The block proportions were precisely made so that the

Table 1: Test specimen geometry. Each was formed from a 50 mm wide strip of 0.12 mm thick age-hardened copper beryllium. The cross-sectional arc-width was $\beta r + 2L = 50$ mm.

Specimen	$\beta(^\circ)$	r (mm)	L (mm)
SR5	69.9	4.8	22.1
SR7	68.8	6.8	20.9
SR8	69.4	7.7	20.3
SR10	69.5	10.1	18.9

Table 2: Finite element model geometry. Each model had an arc-width of 20.5 mm and a thickness of 0.5 mm.

Model	$\beta(^\circ)$	r (mm)	L (mm)
FEA1	60	1	9.71
FEA5	60	5	7.62
FEA10	60	10	5.00
FEA20	60	20	0.00

neutral axis of bending for each strip end was aligned with the rotation axes of the apparatus.

Each end rotation was controlled by manually adjusting dials on the input shafts of the gearboxes, and measured using a vernier scale attached between the torsion gauge and the gearbox. One end of the test apparatus is attached to a carriage, which is free to translate along a low friction track, and the other is fixed against movement.

The strips were bent by increasing the end rotation in increments of 1° and recording the reaction torque. The loading sequence for strip SR5 is shown in Fig. 8 where early torsional buckling is evident. The deformation eventually localised into a central folded region by an end rotation of around 30°. This region clearly propagates outwards from the centre of the strip for larger end rotations. Unloading of the strip was achieved by reversing the direction of rotations to zero again.

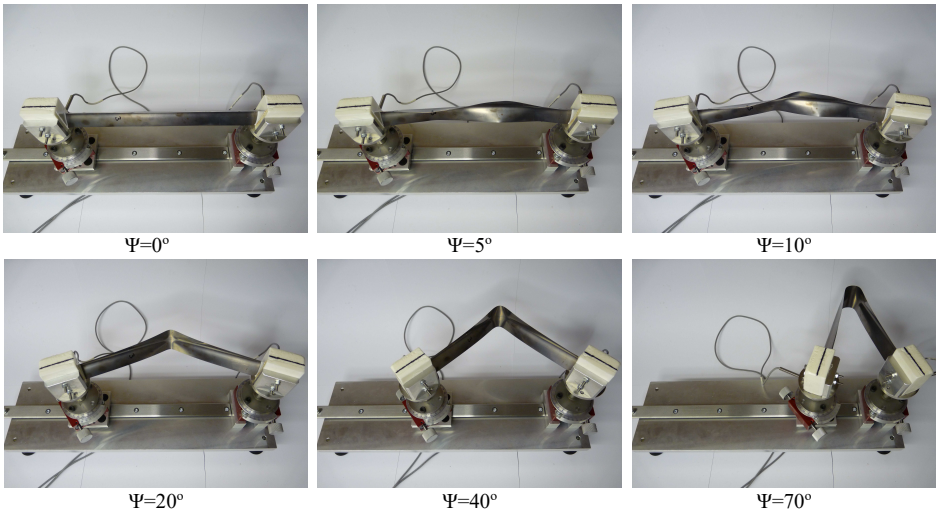

Figure 8: Bending of SR5 creased strip in the forward loading direction. The strip first buckles in a torsional mode before localising into a central folded region around $\Psi = 30°$. Further end rotation is accommodated by propagation of the flattened region outwards from the centre.

4. Finite element analysis

A finite element study over a greater range of geometries was performed using the commercial package ABAQUS [34]. The tested geometries listed in Table 1 used the same linear elastic copper beryllium material properties described in Section 3. Additionally, the geometries shown in Table 2 were modelled with a linear elastic material model with a Young's modulus of 200 GPa, a Poisson's ratio of 0.3, a thickness of 0.5 mm, and a length of 100 mm.

Each strip was rendered as a quarter model, with nodal lines of symmetry along the centreline of the strip and transversely at mid-length. This precludes any torsional deformation but considerably speeds up the simulation; our end point is a localised folded region whose properties, recall, are not affected by the torsional phase.

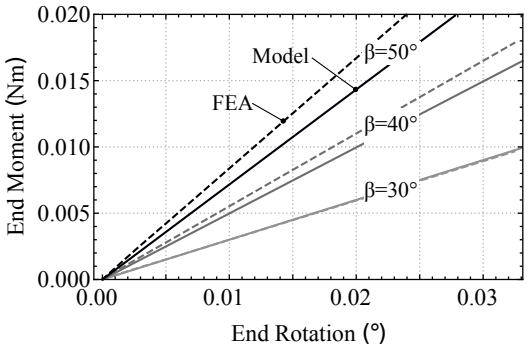

Figure 9: Comparison of the initial elastic response of the analytical and FEA models for a strip with arc-width of 50 mm, $r = 4.8$ mm, and thickness of 0.1 mm. As the sector angle, β, increases the difference between the models also increases due to the shallow curvature assumption for the tape-spring region.

The cross-section at each end was constrained using a rigid-body constraint, with the reference node positioned at the strip centroid. Quadratic, reduced integration, thin shell elements (S8R5) were used to capture the deformation of the crease region more accurately with fewer elements.

A geometrically non-linear static analysis was performed under end-rotation control of the reference nodes, and the reaction moment was recorded. The strip cross-section initially begins to flatten but only in the middle because of the presence of fixed ends. The compressed middle edges are free to buckle locally, which localises the deformation quickly under continued end rotations; much of the remaining strip reverts to the undeformed cross-section connected by transition region. Due to the rapid shape change during this process, an adaptive automatic stabilization scheme was used [34]. The smallest dissipated energy fraction which allowed the analysis to proceed was applied but did not exceed 0.002; the longitudinal radius of curvature at the mid-length was obtained by fitting a circle to five nodes along the deformed centreline of the strip.

A comparison of the initial elastic moment-end rotation behaviour of the FEA and analytical models is shown in Fig. 9. For small end-rotations, and before buckling occurs, the strip deforms to a constant curvature $\kappa = 2\Psi/l$, where Ψ is the end rotation and l is the strip length. Due to the shallow initial curvature assumption for the tape-spring element, the initial stiffness matches closely for small sector angles ($< 30°$) but, as β increases, the difference between the FEA and analytical model increases. This does not have a significant effect on the behaviour in the locally flattened state.

5. Comparison to Experiments

Experiments and finite element analysis are compared in Fig. 10 for the geometries listed in Table 1. There is first a rapid increase in applied moment before torsional buckling occurs, with a good correlation between initial stiffness measurements. Each strip appears to buckle between an end moment of 0.20 and 0.25 Nm at an end rotation in the range 5° to 10°.

The corresponding peak moment from finite element analysis is always larger than the experimentally measured value. This is due to a range of factors, including imposition of symmetry in the finite element model, and the deformation resolution and imperfection sensitivity of the experiments. Recall that predicting the buckling moment of the strip is not a goal of this study.

Continued end rotation leads to the localised folded region and the end moment dropping to an approximately constant value—our proposed propagation moment. From Fig. 8 the localised flattened region has clearly formed by an end rotation of 30°, which is confirmed in Fig. 10. The analytical model

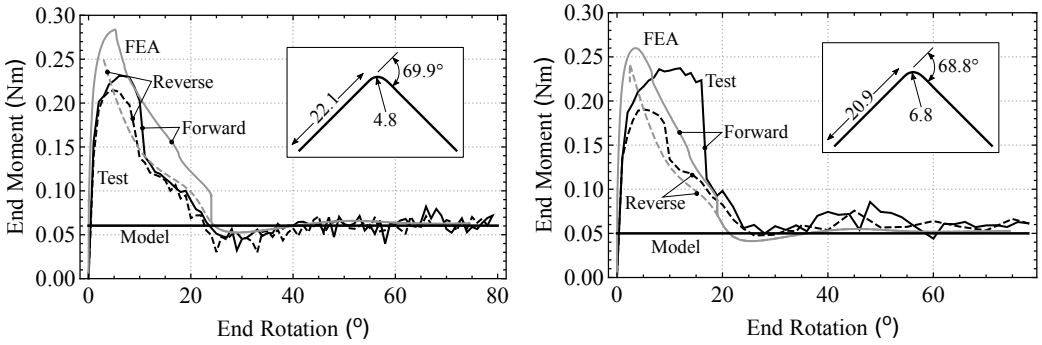

(a) SR5 bending test

(b) SR7 bending test

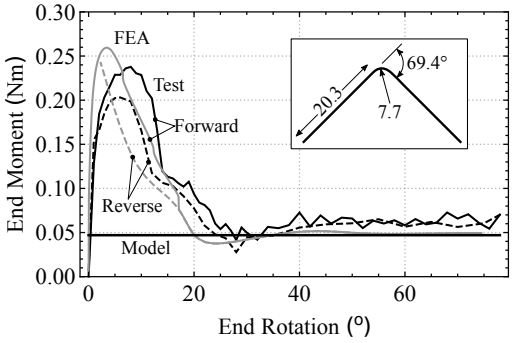

(c) SR8 bending test

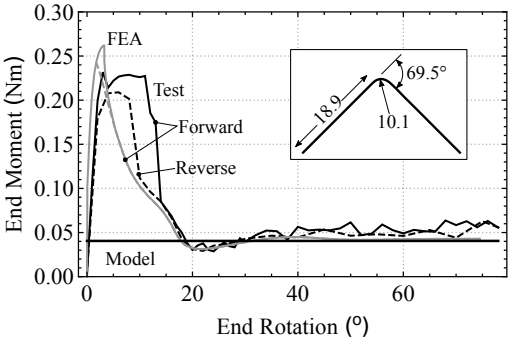

(d) SR10 bending test

Figure 10: Bending test results compared to model predictions. Each strip has a total arc-width $r\beta + 2L = 50$ mm.

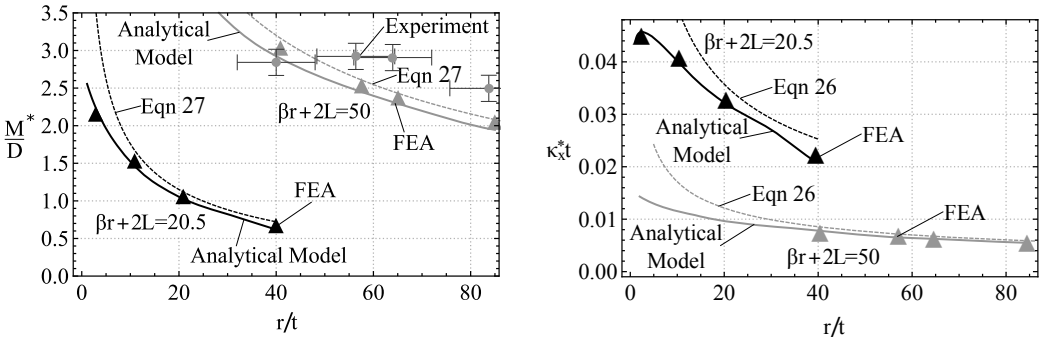

(a) Propagation moment variation with tape-spring r/t ratio.

(b) The propagation curvature variation with tape-spring r/t ratio.

Figure 11: Propagation behaviour of creased strips via analytical model, finite element analysis, and experiments. Experiment and finite element results use the geometry in Tables 1 ($\beta r + 2L = 50$) and 2 ($\beta r + 2L = 20.5$); the analytical results use an average sector angle $\beta = 69.4°$ for the $\beta r + 2L = 50$ mm strips. The approximate expressions for the propagation moment and curvature, given by Eqns 27 and 26 respectively, are shown dashed.

predictions made using Maxwell's construction are also included in Fig. 10, which match the experiments and finite element analysis results well.

During unloading, the moment-end rotation behaviour follows a similar path to the forward direction, with the propagation moment the same as in the forward direction. The peak moment in reverse is however always lower, leading to hysteretic behaviour similar to tape-springs unloading [23].

For larger r/t, the propagation moment, Fig. 11a, and the propagation curvature, Fig. 11b, both decrease. The propagation moments for the finite element and experimental results were obtained by averaging the reaction moment between an end rotation of 30° and 80°. The analytical predictions and finite element model results are in good agreement but the decreasing trend is not as clear in the experimental results. This is due to a combination of factors: there is variability in the cross-sectional geometry, and the

measuring process described in Section 3 results in an approximation of the real cross-section. As shown in Table 1, each test specimen had a different β but the analytical model and finite element results are for $\beta = 69.4°$. The horizontal error bars in Fig. 11a show, for example, a variation of ± 1 mm in the crease radius. Finally, the measurement of the bending moment has some noise, and to obtain the propagation moment, the results were averaged in the plateau region; the vertical error bars show one standard deviation of the data in the plateau region.

The simplified model prediction from Eqn 27 matches the analytical and finite element results well for large tape-spring radii. For smaller radii, however, the simplified model over-predicts the propagation moment, becoming unfeasibly large as the tape radius is reduced to zero: similarly, Eqn 26 increasingly over-predicts the propagation curvature.

The propagation curvature is only compared to finite element analysis in Fig. 11b since the strip curvature could be obtained more reliably. The analytical predictions and finite element results again match very closely.

6. Discussion and conclusions

We have analysed equal-sense bending behaviour of creased strips. Assuming a uniform longitudinal strip curvature, a variational approach was used to obtain the strip deformation as a function of the asymptotic opening angle of its cross-section. The equilibrium cross-sectional shape for a particular strip curvature was obtained by minimising the strip strain energy per unit length with respect to this angle. The model was then interrogated to predict the mechanical behaviour.

As the tape-spring radius is reduced towards the singular limit, the bending resistance increases since smaller creases open less and remain more prominent, thereby increasing the structural depth. Under large deformations, the strip locally flattens to give a cylindrical shape perpendicular to the crease line whose bending resistance and curvature remain approximately constant over a wide range of end rotations. This is relatively insensitive to imperfections and was used to compare the analytical model predictions from Maxwell's construction to experiments and finite element analysis. Very good agreement between all methods has been found, which also validates our assumption of a propagating instability.

A crease is often idealised as a singular torsional spring with a linear stiffness. We have shown that the opening behaviour of a finite-width crease is non-linear but can be reasonably approximated by a singular torsional spring with a linear stiffness of $2D/\beta r$, where D is the flexural rigidity, β is the angle subtended across the crease, and r is the initial crease radius.

Our model provides analysis techniques to enable the use of creased strips where constant curvature tape-springs are commonly used, for example, in deployable structures. Creased strips provide more versatility compared to them because the presence of side panels introduces extra design parameters.

References

[1] J. A. Faber, A. F. Arrieta, A. R. Studart, Bioinspired spring origami, Science 359 (6382) (2018) 1386–1391. doi:10.1126/science.aap7753.

[2] D. J. S. Newman, R. J. Wootton, An Approach to the Mechanics of

Pleating in Dragonfly Wings, Journal of Experimental Biology 125 (1) (1986) 361–372.

[3] H. W. Holdaway, Behavior of Pleated Strips of Wool Fabric in an Extensometer, Textile Research Journal 30 (4) (1960) 296–304. doi:10.1177/004051756003000407.

[4] V. Brunck, F. Lechenault, A. Reid, M. Adda-Bedia, Elastic Theory of Origami-Based Metamaterials, Physical Review E - Statistical, Nonlinear, and Soft Matter Physics 93 (3) (2016) 1–14. doi:10.1103/PhysRevE.93.033005.

[5] F. Guinot, S. Bourgeois, B. Cochelin, L. Blanchard, A Planar Rod Model with Flexible Thin-Walled Cross-Sections. Application to the Folding of Tape Springs, International Journal of Solids and Structures 49 (1) (2012) 73–86. doi:10.1016/j.ijsolstr.2011.09.011.

[6] Ö. Soykasap, Analysis of Tape Spring Hinges, International Journal of Mechanical Sciences 49 (7) (2007) 853–860. doi:10.1016/j.ijmecsci.2006.11.013.

[7] S. Walker, G. Aglietti, A Study of Tape Spring Fold Curvature for Space Deployable Structures, Proceedings of the Institution of Mechanical Engineers, Part G: Journal of Aerospace Engineering 221 (3) (2007) 313–325. doi:10.1243/09544100JAERO209.

[8] K. Seffen, On the Behavior of Folded Tape-Springs, Journal of Applied Mechanics 68 (3) (2001) 369. doi:10.1115/1.1365153.

[9] M. G. Walker, K. A. Seffen, On the Shape of Bistable Creased Strips, Thin-Walled Structures 124 (2018) 538–545. doi:10.1016/j.tws.2017.12.033.

[10] A. Papa, S. Pellegrino, Systematically Creased Thin-Film Membrane Structures, Journal of Spacecraft and Rockets 45 (1) (2008) 10–18. doi:10.2514/1.18285.

[11] K. Woo, K. Nandurkar, C. H. Jenkins, Effective Modulus of Creased Thin Membranes, Journal of Spacecraft and Rockets 45 (1) (2008) 19–26. doi:10.2514/1.29282.

[12] F. Lechenault, B. Thiria, M. Adda-Bedia, Mechanical Response of a Creased Sheet, Physical Review Letters 112 (24) (2014) 244301. doi:10.1103/PhysRevLett.112.244301.

[13] F. Lechenault, M. Adda-Bedia, Generic Bistability in Creased Conical Surfaces, Physical Review Letters 115 (23) (2015) 235501. doi:10.1103/PhysRevLett.115.235501.

[14] J. Dai, F. Cannella, Stiffness Characteristics of Carton Folds for Packaging, Journal of Mechanical Design 130 (2) (2008) 022305. doi:10.1115/1.2813785.

[15] K. Francis, J. Blanch, S. Magleby, L. Howell, Origami-Like Creases in Sheet Materials for Compliant Mechanism Design, Mechanical Sciences 4 (2) (2013) 371–380. doi:10.5194/ms-4-371-2013.

[16] C. Pradier, J. Cavoret, D. Dureisseix, C. Jean-Mistral, F. Ville, An Experimental Study and Model Determination of the Mechanical Stiffness

of Paper Folds, Journal of Mechanical Design 138 (4) (2016) 041401. doi:10.1115/1.4032629.

[17] M. Dias, B. Audoly, A Non-Linear Rod Model for Folded Elastic Strips, Journal of the Mechanics and Physics of Solids 62 (2014) 57–80. doi:10.1016/j.jmps.2013.08.012.

[18] M. Dias, L. Dudte, L. Mahadevan, C. Santangelo, Geometric Mechanics of Curved Crease Origami, Physical Review LettersDias, M. A., Dudte, L. H., Mahadevan, L., & Santangelo, C. D. (2012). Geometric Mechanics of Curved Crease Origami. Physical Review Letters, 109(11), 114301. https://doi.org/10.1103/PhysRevLett.109.114301 109 (11) (2012) 114301. doi:10.1103/PhysRevLett.109.114301.

[19] E. Mansfield, Large-Deflexion Torsion and Flexure of Initially Curved Strips, Proceedings of the Royal Society A: Mathematical, Physical and Engineering Sciences 334 (1598) (1973) 279–298. doi:10.1098/rspa.1973.0092.

[20] L. G. Brazier, On the Flexure of Thin Cylindrical Shells and Other "thin" Sections, Proceedings of the Royal Society A: Mathematical, Physical and Engineering Sciences 116 (773) (1927) 104–114. doi:10.1098/rspa.1927.0125.

[21] L. Mahadevan, A. Vaziri, M. Das, Persistence of a Pinch in a Pipe, Europhysics Letters (EPL) 77 (4) (2007) 40003. doi:10.1209/0295-5075/77/40003.

[22] T. Barois, L. Tadrist, C. Quilliet, Y. Forterre, How a Curved Elastic Strip Opens, Physical Review Letters 113 (21) (2014) 1–5. doi:10.1103/PhysRevLett.113.214301.

[23] K. Seffen, S. Pellegrino, Deployment Dynamics of Tape Springs, Proceedings of the Royal Society A: Mathematical, Physical and Engineering Sciences 455 (1983) (1999) 1003–1048. doi:10.1098/rspa.1999.0347.

[24] C. Calladine, Theory of Shell Structures, Cambridge University Press, Cambridge, 1983.

[25] Wolfram Research Inc, Mathematica, Version 11, 2017.

[26] M. Walker, Flexural Mechanics of Creased Thin Metallic Strips, PhD dissertation. University of Cambridge. Cambridge, UK., 2018. doi:10.17863/CAM.24199.

[27] M. Walker, K. Seffen, The Mechanics of Metallic Folds, in: R. Lang, M. Bolitho, Z. You (Eds.), 7th International Meeting on Origami in Science, Mathematics and Education, Oxford, UK, 2018.

[28] E. Chater, J. Hutchinson, On the Propagation of Bulges and Buckles, Journal of Applied Mechanics 51 (2) (1984) 269–277.

[29] S. Kamalarasa, C. R. Calladine, Buckle Propagation in Submarine Pipelines, International Journal of Mechanical Sciences 30 (3-4) (1988) 217–228. doi:10.1016/0020-7403(88)90056-2.

[30] S. Kyriakides, R. Arseculeratne, Propagating Instabilities in Long Shal-

low Panels, Journal of Engineering Mechanics 119 (3) (1993) 570–583. doi:10.1061/(ASCE)0733-9399(1993)119:3(570).

[31] K. Chater, E., Hutchinson, J.W., Neale, Buckle Propagation on a Beam on a Nonlinear Elastic Foundation, in: G. Thompson, J.M.T., Hunt (Ed.), Collapse, Cambridge University Press, 1983, pp. 31–41.

[32] K. A. Seffen, Progressive Collapse of the World Trade Center: Simple Analysis, Journal of Engineering Mechanics 134 (2) (2008) 125–132. doi:10.1061/(ASCE)0733-9399(2008)134:2(125).

[33] S. Kyriakides, Propagating Instabilities in Structures, in: Advances in Applied Mechanics, Volume 30, Academic Press, Boston, MA, 1993, pp. 67–189. doi:10.1016/S0065-2156(08)70174-1.

[34] Dassault Systèmes, Abaqus/CAE User's Guide, Providence, RI, USA., 2014.